A Dual Fluorescence and NMR Study for the Interaction Between Xanthene Dyes and Nanoparticles

Hui Xu and Leah B. Casabianca*

Department of Chemistry

Clemson University, Clemson, SC 29634 USA

*corresponding author, lcasabi@clemson.edu

Abstract

Fluorescent dyes and nanoparticles (NPs) have been widely used together to make novel biosensors, taking advantage of their unique characteristics. It is crucial to have techniques that enable us to gain detailed and high-resolution information regarding the interaction between nanoparticles and fluorescent dyes. In this work, we chose rhodamine B (RhB) and amidine- and carboxylate-modified polystyrene (CML) nanoparticles as models and employed both NMR (¹H and STD NMR) and optical (UV-Vis and fluorescence) techniques to investigate the interaction between nanoparticles and fluorescent dyes. From UV-Vis and fluorescence spectroscopy, we see that there are larger red shifts when rhodamine B binds to carboxylate modified polystyrene nanoparticles than amidine modified nanoparticles. Correspondingly, RhB has broader NMR peaks and a larger STD effect when binding to CML NPs than amidine NPs. Results from these two techniques validate each other. It is notable that the NMR techniques provide more reliable data than UV-Vis and fluorescence methods. Moreover, we show that NMR techniques, especially STD NMR, can provide more atomic-level binding geometry information. The higher STD effect of the smaller aromatic ring of RhB implies that this aromatic ring is closer to the surface of nanoparticles when binding to polystyrene nanoparticles.

Introduction

Xanthenes, an important type of fluorophore, have gained extensive attention from academic researchers and industries due to their remarkable photophysical properties, such as high photostability, excellent quantum yield and high molar extinction coefficient. ^{1,2} One of these popular xanthene fluorophores, rhodamine, has been widely developed because of its unique fluorescent properties. Non-fluorescent and colorless rhodamine spirolactam or spirolactone derivatives will change color to pink and emit fluorescence once the spirolactam/lactone ring is opened. ^{1,3,4} Researchers have taken advantage of this characteristic and applied rhodamine and its related derivatives to many fields, including applications in biological makers and bioimaging. ^{5–8} For instance, rhodamine derivatives have been extensively used as fluorescent chemosensors to sense biologically and environmentally-related metal ions (Cu²⁺, Hg²⁺, Zn²⁺, Pd²⁺ etc), ^{9–11} to detect pH^{12,13} and to monitor enzyme activity. ^{14–16} Compared with other sensing methods, fluorescent probes can be easily introduced into the system and are highly sensitive and selective. ¹ For these reasons, fluorescence imaging is excellent in providing real time imaging in cells. ^{2,17} In this work, we use an inexpensive rhodamine dye, rhodamine B (RhB), as a model for xanthene dyes because its derivatives have been extensively applied in many areas. ^{9,10,18}

Due to their unique physicochemical properties, nanoparticles (NPs) are important in the biomedical field. To date, nanoparticles have been used in drug delivery, bioimaging and as biosensors. 19-22 Recently, significant effort has been made to develop biosensors by taking advantage of both nanoparticles and fluorescent dyes. For example, optical oxygen sensors have been developed by trapping fluorescent dyes inside a polymer nanoparticle. Wang et al²³ have utilized amino-modified polystyrene beads to encapsulate dyes and Pt coordination complexes as oxygen probes to determine and image the intracellular oxygen levels. The McNeill group has developed single nanoparticle oxygen sensors by using conjugated polymer nanoparticles to entrap an oxygen sensitive dye, platinum(II) octaethylporphine.²⁴ The function of NPs mainly relies on how their surface interacts with other molecules and their surroundings.²⁵ One key element to the development of nanoparticle-dye sensors is the understanding of nanoparticle-dye interaction. which requires a powerful characterization method. The main characterization techniques that are currently used are fluorescence spectroscopies, which are mainly based on the fluorescence response. Fluorescence, however, cannot provide atomic-level details regarding nanoparticle-dye interactions. Hence, a technique that enables us to obtain detailed and high-resolution information about the interaction between NPs and dyes is crucial to the development of better biosensors.

In recent years, various Nuclear Magnetic Resonance (NMR) spectroscopy experiments have been developed to gain insight into structural information regarding small molecules and proteins on the surface of nanoparticles.^{26–38} NMR experiments are non-destructive and can provide atomic-level resolution. These experiments include measuring diffusion coefficients^{28,30} of free and bound ligands using either pulsed-field gradient or diffusion-ordered spectroscopy (DOSY) experiments, exploiting the different relaxation times in free and bound ligands^{29-31,34-37}, methods that exploit different rotational correlation times between the small ligand and large receptor such

as NOESY30 and waterLOGSY39,40, and methods that rely on saturation transfer such as saturation-transfer difference (STD)-NMR³⁰ and dark-state exchange saturation transfer (DEST)^{26,31,38}. STD-NMR^{41,42} is particularly effective to probe ligand binding on a nanoparticle surface. 43-48 In each STD-NMR experiment, two spectra, one on-resonance and one offresonance spectrum, are collected. The difference between these two spectra is the location of the saturation frequency. The off-resonance spectrum is acquired with saturation at a frequency where neither receptor (nanoparticles in this work) nor ligand (dyes) would resonate. In the onresonance spectrum, however, saturation is at a frequency where only receptors will resonate. This selective saturation will subsequently spread throughout the entire network of receptor protons through spin diffusion. When the ligands bind to receptor pockets, they will receive part of the saturation transferred from the receptor. Since the binding is dynamic, the bound ligand will exchange with the free ligands during the saturation period, leading to a reduction of the ligand peak intensity. Subtracting the on-resonance spectrum from the off-resonance spectrum gives the difference spectrum that contains peaks only from binding ligands. DEST is another common NMR method used to investigate surface interactions. 49,50 The DEST experiment is used in particular to characterize visible species that are in exchange with a dark state, which is rendered NMR-invisible due to slow tumbling resulting in large transverse relaxation rates. It is notable that unlike STD, the DEST method does not require saturation transfer from receptors to ligands via cross-relaxation.

These NMR techniques come with limitations, the main one being the inherent low sensitivity of the NMR technique. This requires higher concentrations of sample than corresponding optical techniques, and the higher concentrations required for NMR will influence binding equilibria. However, the strength in these NMR techniques is the atomic-level information about binding geometry that they are able to provide. STD-NMR, for example, can be used for epitope mapping. All other things being equal, a higher STD effect will be observed for protons on a ligand that are closer to the receptor in the bound geometry.

In this work, the interaction between RhB dye and two kinds of polystyrene nanoparticles (carboxylate-modified and amidine-modified) was determined by ¹H and STD NMR spectroscopy. Additionally, we also measure UV-Vis and fluorescence spectroscopy to validate the NMR results. Conclusions from these two techniques are in line with each other. However, we find that the NMR techniques are more reliable as indicated by a lower percent error in repeat measurements.

Methods

Amidine polystyrene latex beads (4% w/v suspension in deionized water, 0.02 µm) and carboxylate-modified (CML) polystyrene latex beads (4% w/v suspension in deionized water, 0.02 µm) were purchased from Thermo Fisher Scientific (Waltham, MA, USA). Rhodamine B (≥95%, HPLC) was purchased from Sigma-Aldrich (St. Louis, MO). Hydrochloric acid, sodium hydroxide and deuterium oxide (99.8 atom % D, for NMR, Acros Organics) were purchased from Fisher Scientific (Hampton, NH, USA). All reagents and solvents were used as received. Deionized water was prepared using a Millipore Milli-Q purifier.

NMR samples consisted of 1mM RhB and 11 nM polystyrene NPs in D_2O . The total volume of solution was 1 mL. 5mm od NMR tubes (Norell inc, Morganton, NC) were used in all NMR experiments. For UV-Vis and fluorescence experiments, samples consisted of 1 uM RhB and 0.5 uM polystyrene NPs in H_2O . The final volume was 3 mL. The pH of all samples was adjusted to 7 by addition of a minimum amount of HCl and NaOH solutions. The pH values were directly measured by the pH probe, without any corrections for isotope effect.

The UV-Visible (UV-Vis) absorption spectra were recorded on an Agilent 8453 UV-Vis spectrophotometer. Plastic cuvettes with 10 mm path length are used to hold samples. A blank sample with corresponding solvent only was measured at the beginning of each set of samples. The spectrum was measured over the range 200-1000 nm. The fluorescence spectra were recorded with a commercial fluorometer (Quantamaster, PTI, Inc.). The excitation wavelength was 540 nm. The emission spectra were measured from 525 to 700 nm. All NMR experiments were performed on a Bruker 500 MHz NEO NMR spectrometer with a BBO Prodigy nitrogencooled cryoprobe. ¹H experiments were acquired with 3-second acquisition time, 8 scans, 1s recycle delay and 12 ppm spectral width. STD experiments were performed using the standard Bruker pulse sequence "stddiffesgp", 41,42 where a train of 50 ms Gaussian pulses at a power of 7.8 mW (0.46 kHz) was used to achieve saturation. Off-resonance saturation was performed at 40 ppm and on-resonance saturation was performed at 12 ppm. The on- and off-resonance spectra were collected in an interleaved manner. The STD experiment was acquired with 3 s acquisition time, 128 scans, 4 dummy scans and 12 ppm spectral width. For both 1D ¹H and STD experiments, the excitation sculpting with gradients water suppression sequence was used.51 All experiments were done at 298K. Bruker Topspin 4.0.6 software was used to process all NMR spectra. A custom-written MATLAB script was used to process phase corrected spectra to calculate peak integrals. All MATLAB operations were done with MATLAB R2018a software (MathWorks, Natick, MA, USA).

Results and Discussion

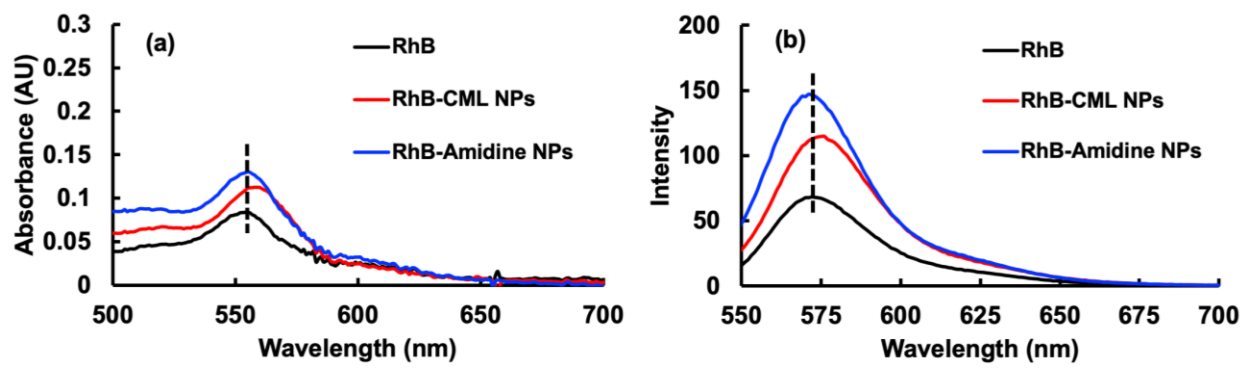


Figure 1. UV-Vis absorption (a) and fluorescence emission (b) spectra of RhB, RhB-CML NPs and RhB-Amidine NPs at pH 7. The baseline of RhB-amidine NPs in the UV spectrum has been adjusted for clarity. The intensity of the fluorescence spectrum (y axis) is divided by 1000.

Representative UV-Vis absorbance and fluorescence emission spectra of RhB samples are shown in Figure 1. In Figure 1a, the RhB maximum of absorbance (λmax) at pH 7 is 555 nm. The

absorbance band of RhB (λmax = 555 nm) does not shift at all when RhB interacts with amidine modified nanoparticles (0.75 ± 0.95 nm). On the contrary, the presence of carboxylate modified polystyrene nanoparticles causes prominent red shifts of RhB (3.5 ± 1.7 nm), reaching a λmax of 558nm. UV-Vis spectroscopy is primarily used for detecting environmental change. The red-shift of the maximum absorbance peak is due to the adsorption of RhB to the surface of nanoparticles. Similar red-shift phenomenon has been reported in the literature for the binding of RhB to polymers. By comparing the two nanoparticles, we can see an indication that RhB binds to CML NPs, whereas the binding to amidine NPs is negligible.

In order to confirm this, fluorescence experiments were performed. Figure 1b illustrates the influence of nanoparticles on RhB. The maximum emission of the Rhodamine B was at 572 nm. Red-shifts of 2.3 ± 1.5 nm are observed when RhB interacts with CML NPs while a 0.5 ± 0.57 nm blue-shift is seen for amidine NPs. Similar red-shift of fluorescence emission peak is reported in the literature for RhB with polystyrene nanoparticles. This peak shift indicates that RhB indeed binds to CML nanoparticles. The electronic environment of RhB is affected by interactions with NPs, which resulted in an emission peak shift. Interestingly, the emission peak has a different shift range when interacting with different modified surface NPs. The larger peak shift of RhB with CML NPs than amidine NPs implies that RhB binds to CML NPs, but not to amidine NPs, which is in line with the UV-Vis results. This can be attributed to the electrostatic attraction between the negatively charged carboxylate group on the surface of CML NPs and positively charged amino group of RhB molecules. However, there is no such attraction between positively charged RhB and neutral amidine NPs.

Results for individual trials of UV-Vis and fluorescence experiments are listed in Table S1 of the supporting information. Although these optical spectroscopy techniques have been used in the past to explore binding, this might not be the best method to use to study RhB binding to polystyrene NPs, since the peak shifts are small and have a large variability. In addition, the absorbance peak and emission peak of RhB overlap with the tail of the NP scattering feature (shown in Figure S1 in the supporting information), further complicating the analysis. However, the maximum of the RhB peak position does not appear to be influenced by the presence of the NP scattering feature.

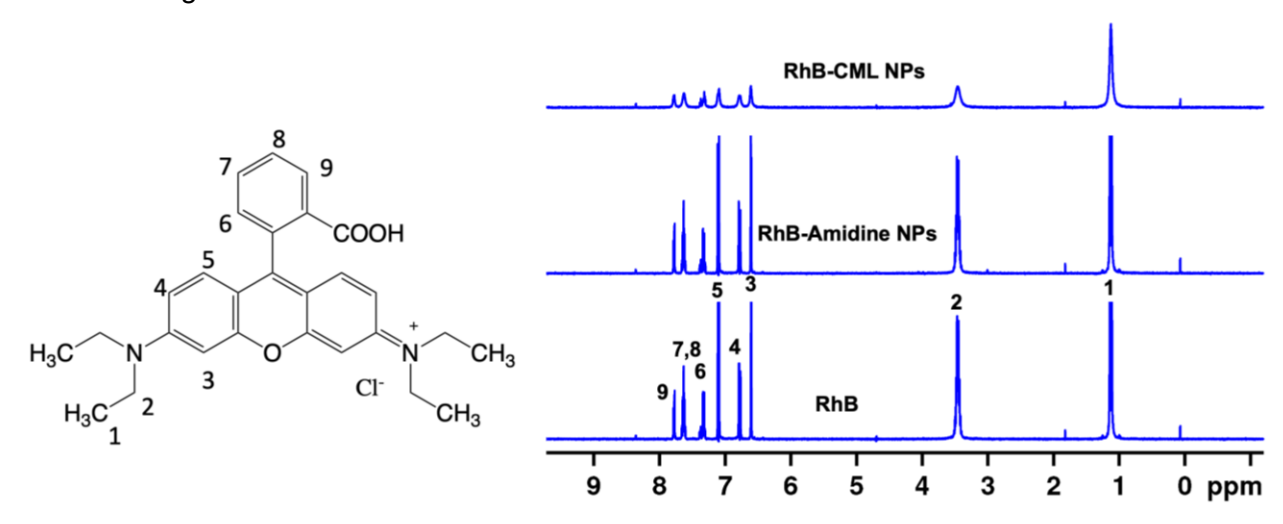


Figure 2. RhB molecular structure, its peak assignment and ¹H NMR spectra of 1mM RhB, RhB-amidine NPs and RhB-CML NPs at pH 7.

To provide more reliable insight into RhB binding to polystyrene NPs, as well as obtain structural information, we used NMR techniques. Figure 2 displays the 1D ¹H NMR spectrum of RhB and its peak assignment based on COSY, NOESY and HSQC experiments. An expanded ¹H NMR spectrum between 6 ppm and 8 ppm is shown in Figure S2 in the supporting information. From the bottom to the top are spectra of RhB only, RhB with amidine modified polystyrene NPs and RhB with carboxylate modified polystyrene NPs. Comparing these spectra, proton peaks are sharp and have high intensity for the sample containing only RhB, and are broadened when RhB is combined with nanoparticles. In the case of amidine NPs, the peak shape and intensity are similar to those of RhB only samples. Interacting with CML NPs, however, RhB line broadening is more pronounced and a large decrease in intensity is observed. This is due to the slow tumbling rate of polystyrene NPs. As the size of NPs is large, their tumbling rate is slow in solution and thus leads to fast T₂ relaxation. The increased transverse relaxation rate mainly contributes to the line broadening of peaks. Therefore, when RhB molecules bind to the surface of NPs, they will have similar tumbling rate as NPs, resulting in line broadening and decreased peak intensity. Notably, the different line broadening effect on RhB peaks between CML NPs and amidine NPs implies that RhB prefers to bind to CML NPs instead of amidine NPs. The relative peak integral intensities for each spectrum are listed in Table S2 in the supporting information. The reduction in peak integral intensity when RhB binds to CML NPs indicates that a fraction of the RhB is bound tightly to the nanoparticles. In contrast, no decrease in peak integral intensity is observed when RhB is combined with amidine NPs. Taken together, the 1D proton NMR data agrees with the UV-Vis and fluorescence spectra, indicating binding between RhB and CML NPs, and weak or nonexistent binding between RhB and amidine NPs.

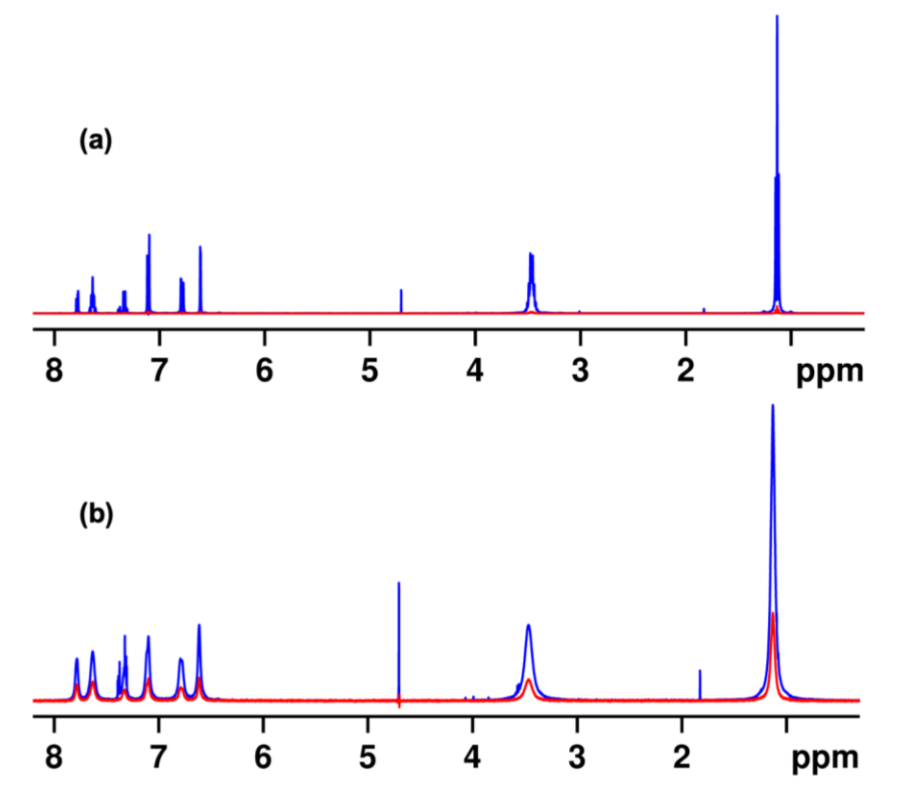


Figure 3. STD reference (blue) and difference (red) spectra of 1 mM RhB with Amidine NPs (a) and CML NPs (b) at pH 7. The on- and off- resonance spectra are saturated at 12 ppm and 40 ppm, respectively. The saturation times and recycle delays are 2.5 s and 3 s for CML NPs and 3.5 s and 4 s for amidine NPs.

The STD NMR spectra of RhB interacting with amidine and CML polystyrene nanoparticles are shown in Figure 3. The blue line is the reference spectrum while the red line represents the difference spectrum. When RhB is mixed with amidine NPs, the STD effect is nearly not observable, as shown in Figure 3a. On the other hand, there is a significant large STD effect when RhB interacts with the carboxylate modified polystyrene nanoparticles in Figure 3b. The larger STD effect again indicates that stronger binding exists between RhB and CML NPs than RhB and amidine NPs.

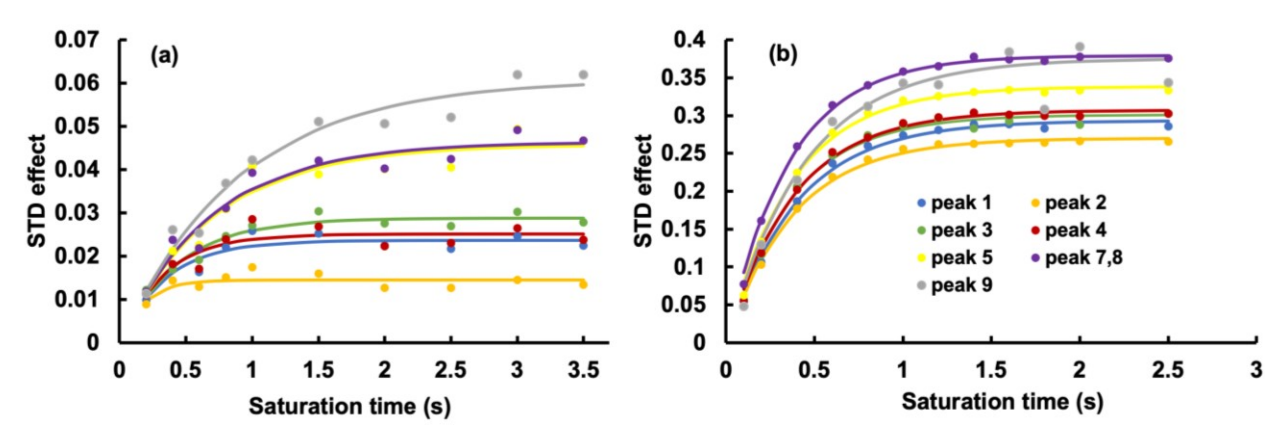


Figure 4. STD buildup curve of RhB-amidine NPs (a) and RhB-CML NPs (b) at pH 7. The dots are experimental data and the lines are the best fit to $S(t) = S_{max}$ (1-e-kt), where S(t) is the STD effect at time t, S_{max} is the maximum STD effect and k is a buildup time constant. The STD effect of peak 6 is not displayed due to peak overlap with impurities.

A series of STD experiments with different saturation times was collected. The STD effect of each peak, which is defined as the peak intensity in the difference spectrum divided by that in the reference spectrum, is calculated and plotted as a function of saturation time to make the full STD buildup curves as shown in Figure 4. The maximum STD effect of RhB-CML NPs is around 0.4, which is 7 times larger than that of RhB-amidine NPs (0.06). The much higher STD effect of RhB-CML NPs implies the stronger binding between RhB and CML NPs. RhB molecules receive more saturation transferred from nanoparticles if they bind more strongly to nanoparticles, leading to higher peak intensity in the difference spectrum and thus a larger STD effect. This is consistent with ¹H NMR, UV-Vis and fluorescence spectra.

Figure 5. RhB molecular structure with the maximum STD effect of RhB-CML NPs displayed beside each peak. The STD effect of peak 6 is not displayed due to peak overlap with impurities.

In addition to giving information about relative binding affinity as the optical methods mentioned above, STD-NMR can also provide insight into the binding geometry of RhB on the surface of polystyrene nanoparticles. As displayed in Figure 5, the maximum STD effect of the aliphatic protons (peak 1 and 2) of RhB is smaller than that of aromatic groups (peaks 3-9). This can be attributed to the strong $\pi-\pi$ interaction between aromatic rings of RhB molecules and phenyl groups of polystyrene in the NPs. A previous study explored the influence of stacking of RhB on polymers containing aromatic rings by using polymers with and without aromatic rings. ⁵⁴ Interestingly, the STD effect of peaks 7-9 from the small aromatic ring is larger than that of aromatic peaks 3-5 from the large aromatic ring. This provides more detailed structural information for RhB binding to nanoparticles. That is, the small aromatic ring of RhB is closer to the surface of nanoparticles when binding to polystyrene nanoparticles. We speculate that this might be associated with the steric effect of the large aromatic ring and bulky ethylamine groups, which makes it harder for this aromatic ring to get close to the aromatic rings in the nanoparticles.

The STD-NMR experiments were repeated 4 times and the average and standard deviation of the STD effects are shown in Tables S3 and S4 of the supporting information. The percent error in the STD-NMR measurements is much less than that of the UV-Vis and fluorescence experiments. Although all three techniques lead to similar conclusions and validate each other, the NMR technique is more reliable when studying RhB interacting with polystyrene NPs.

Conclusions

In this work, we have utilized both NMR (¹H and STD NMR) and optical (UV-Vis and fluorescence) techniques to investigate the interaction between the xanthene dye RhB and two different functionalized polystyrene nanoparticles. From UV-Vis and fluorescence spectroscopy, we see that there are larger red shifts when RhB binds to carboxylate modified NPs than amidine modified NPs. Correspondingly, RhB has broader peaks and a larger STD effect when binding to CML NPs than amidine NPs from the NMR spectra. Results from these two techniques validate each other, but the NMR techniques provide more reliable data, according to the percent error in the measurements, than UV-Vis and fluorescence methods. Moreover, we show that NMR techniques, especially STD-NMR, can provide atomic-level binding geometry information.

Supporting Information

Average and standard deviation of the maximum UV-Vis absorbance, fluorescence emission peak shift, and maximum STD effect; table of NMR peak integrals; expanded 1H NMR spectrum between 6 ppm and 8 ppm; and UV-Vis spectra and fluorescence spectra of nanoparticles alone.

Acknowledgements

We thank Prof. Jason McNeill for helpful discussions. We thank the NSF (CHE-1751529 and CHE-1725919) for support of this research. Acknowledgement is made to the Donors of the American Chemical Society Petroleum Research Fund for partial support of this research (Grant 58738-DNI6).

References

- (1) Chen, X.; Pradhan, T.; Wang, F.; Kim, J. S.; Yoon, J. Fluorescent Chemosensors Based on Spiroring-Opening of Xanthenes and Related Derivatives. *Chem. Rev.* **2012**, *112* (3), 1910–1956. https://doi.org/10.1021/cr200201z.
- (2) Kushida, Y.; Nagano, T.; Hanaoka, K. Silicon-Substituted Xanthene Dyes and Their Applications in Bioimaging. *The Analyst* **2015**, *140* (3), 685–695. https://doi.org/10.1039/C4AN01172D.
- (3) Santos-Figueroa, L. E.; Moragues, M. E.; Climent, E.; Agostini, A.; Martínez-Máñez, R.; Sancenón, F. Chromogenic and Fluorogenic Chemosensors and Reagents for Anions. A Comprehensive Review of the Years 2010–2011. *Chem. Soc. Rev.* **2013**, *42* (8), 3489–3613. https://doi.org/10.1039/C3CS35429F.
- (4) Dujols, V.; Ford, F.; Czarnik, A. W. A Long-Wavelength Fluorescent Chemodosimeter Selective for Cu(II) Ion in Water. *J. Am. Chem. Soc.* **1997**, *119* (31), 7386–7387. https://doi.org/10.1021/ja971221g.
- (5) Liu, C.; Jiao, X.; Wang, Q.; Huang, K.; He, S.; Zhao, L.; Zeng, X. A Unique Rectilinearly π-Extended Rhodamine Dye with Large Stokes Shift and near-Infrared Fluorescence for Bioimaging. *Chem. Commun.* **2017**, *53* (77), 10727–10730. https://doi.org/10.1039/C7CC06220F.
- (6) Qian, X.; Xu, Z. Fluorescence Imaging of Metal Ions Implicated in Diseases. *Chem. Soc.*

- Rev. 2015, 44 (14), 4487-4493. https://doi.org/10.1039/C4CS00292J.
- (7) Shulov, I.; Oncul, S.; Reisch, A.; Arntz, Y.; Collot, M.; Mely, Y.; S. Klymchenko, A. Fluorinated Counterion-Enhanced Emission of Rhodamine Aggregates: Ultrabright Nanoparticles for Bioimaging and Light-Harvesting. *Nanoscale* **2015**, *7* (43), 18198–18210. https://doi.org/10.1039/C5NR04955E.
- (8) Wang, L.; Du, W.; Hu, Z.; Uvdal, K.; Li, L.; Huang, W. Hybrid Rhodamine Fluorophores in the Visible/NIR Region for Biological Imaging. *Angew. Chem. Int. Ed.* **2019**, *58* (40), 14026–14043. https://doi.org/10.1002/anie.201901061.
- (9) Chen, Y.; Chen, B.; Han, Y. A Novel Rhodamine-Based Fluorescent Probe for the Fluorogenic and Chromogenic Detection of Pd2+ Ions and Its Application in Live-Cell Imaging. Sens. Actuators B Chem. 2016, 237, 1–7. https://doi.org/10.1016/j.snb.2016.06.067.
- (10) Jiao, Y.; Zhou, L.; He, H.; Yin, J.; Gao, Q.; Wei, J.; Duan, C.; Peng, X. A Novel Rhodamine B-Based "off-on" Fluorescent Sensor for Selective Recognition of Copper (II) Ions. *Talanta* **2018**, *184*, 143–148. https://doi.org/10.1016/j.talanta.2018.01.073.
- (11) Erdemir, S.; Yuksekogul, M.; Karakurt, S.; Kocyigit, O. Dual-Channel Fluorescent Probe Based on Bisphenol A-Rhodamine for Zn2+ and Hg2+ through Different Signaling Mechanisms and Its Bioimaging Studies. *Sens. Actuators B Chem.* **2017**, *241*, 230–238. https://doi.org/10.1016/j.snb.2016.10.082.
- (12) Lee, D.; Swamy, K. M. K.; Hong, J.; Lee, S.; Yoon, J. A Rhodamine-Based Fluorescent Probe for the Detection of Lysosomal PH Changes in Living Cells. *Sens. Actuators B Chem.* **2018**, *266*, 416–421. https://doi.org/10.1016/j.snb.2018.03.133.
- (13) Shen, S.-L.; Chen, X.-P.; Zhang, X.-F.; Miao, J.-Y.; Zhao, B.-X. A Rhodamine B-Based Lysosomal PH Probe. *J. Mater. Chem. B* **2015**, *3* (5), 919–925. https://doi.org/10.1039/C4TB01763C.
- (14) Lorey, S., Faust, J., Mrestani-Klaus, C., Kähne, T., Ansorge, S., Neubert, K., & Bühling, F. Transcellular Proteolysis Demonstrated by Novel Cell Surface-Associated Substrates of Dipeptidyl Peptidase IV (CD26). *J. Biol. Chem.* 2002, 277 (36), 33170–33177. https://doi.org/10.1074/jbc.m200798200.
- (15) Yatzeck, M. M.; Lavis, L. D.; Chao, T.-Y.; Chandran, S. S.; Raines, R. T. A Highly Sensitive Fluorogenic Probe for Cytochrome P450 Activity in Live Cells. *Bioorg. Med. Chem. Lett.* **2008**, *18* (22), 5864–5866. https://doi.org/10.1016/j.bmcl.2008.06.015.
- (16) Li, J.; Petrassi, H. M.; Tumanut, C.; Masick, B. T.; Trussell, C.; Harris, J. L. Substrate Optimization for Monitoring Cathepsin C Activity in Live Cells. *Bioorg. Med. Chem.* **2009**, 17 (3), 1064–1070. https://doi.org/10.1016/i.bmc.2008.02.002.
- (17) Hemmerich, P. H.; Mikecz, A. H. von. Defining the Subcellular Interface of Nanoparticles by Live-Cell Imaging. *PLOS ONE* **2013**, *8* (4), e62018. https://doi.org/10.1371/journal.pone.0062018.
- (18) Poon, C. K.; Tang, O.; Chen, X.-M.; Kim, B.; Hartlieb, M.; Pollock, C. A.; Hawkett, B. S.; Perrier, S. Fluorescent Labeling and Biodistribution of Latex Nanoparticles Formed by Surfactant-Free RAFT Emulsion Polymerization. *Macromol. Biosci.* **2017**, *17* (10), 1600366. https://doi.org/10.1002/mabi.201600366.
- (19) Khan, I.; Saeed, K.; Khan, I. Nanoparticles: Properties, Applications and Toxicities. *Arab. J. Chem.* **2019**, *12* (7), 908–931. https://doi.org/10.1016/j.arabjc.2017.05.011.
- (20) Anselmo, A. C.; Mitragotri, S. Nanoparticles in the Clinic. *Bioeng. Transl. Med.* **2016**, *1* (1), 10–29. https://doi.org/10.1002/btm2.10003.
- (21) McNamara, K.; Tofail, S. A. M. Nanoparticles in Biomedical Applications. *Adv. Phys. X* **2017**, *2* (1), 54–88. https://doi.org/10.1080/23746149.2016.1254570.
- (22) Kim, H. W.; Kim, J. W.; Jo, S. H.; Lee, C.-L.; Lee, W.-K.; Park, S. S.; Chung, B.; Yoo, S. I. PH-Responsive Assembly of Metal Nanoparticles and Fluorescent Dyes by Diblock Copolymer Micelles. *Soft Matter* **2015**, *11* (22), 4402–4407.

- https://doi.org/10.1039/C5SM00824G.
- (23) Wang, X.; H. Gorris, H.; A. Stolwijk, J.; J. Meier, R.; M. Groegel, D. B.; Wegener, J.; S. Wolfbeis, O. Self-Referenced RGB Colour Imaging of Intracellular Oxygen. *Chem. Sci.* **2011**, *2* (5), 901–906. https://doi.org/10.1039/C0SC00610F.
- (24) Wu, C.; Bull, B.; Christensen, K.; McNeill, J. Ratiometric Single-Nanoparticle Oxygen Sensors for Biological Imaging. *Angew. Chem. Int. Ed.* **2009**, *48* (15), 2741–2745. https://doi.org/10.1002/anie.200805894.
- (25) Loos, C.; Syrovets, T.; Musyanovych, A.; Mailänder, V.; Landfester, K.; Nienhaus, G. U.; Simmet, T. Functionalized Polystyrene Nanoparticles as a Platform for Studying Bio–Nano Interactions. *Beilstein J. Nanotechnol.* **2014**, *5*, 2403–2412. https://doi.org/10.3762/bjnano.5.250.
- (26) Egner, T. K.; Naik, P.; Nelson, N. C.; Slowing, I. I.; Venditti, V. Mechanistic Insight into Nanoparticle Surface Adsorption by Solution NMR Spectroscopy in an Aqueous Gel. *Angew. Chem.* **2017**, *129* (33), 9934–9938. https://doi.org/10.1002/ange.201704471.
- (27) Assfalg, M.; Ragona, L.; Pagano, K.; D'Onofrio, M.; Zanzoni, S.; Tomaselli, S.; Molinari, H. The Study of Transient Protein–Nanoparticle Interactions by Solution NMR Spectroscopy. *Biochim. Biophys. Acta BBA Proteins Proteomics* **2016**, *1864* (1), 102–114. https://doi.org/10.1016/j.bbapap.2015.04.024.
- (28) Glaria, A.; Cure, J.; Piettre, K.; Coppel, Y.; Turrin, C.-O.; Chaudret, B.; Fau, P. Deciphering Ligands' Interaction with Cu and Cu2O Nanocrystal Surfaces by NMR Solution Tools. *Chem. Eur. J.* **2015**, *21* (3), 1169–1178. https://doi.org/10.1002/chem.201403835.
- (29) Wu, M.; Vartanian, A. M.; Chong, G.; Pandiakumar, A. K.; Hamers, R. J.; Hernandez, R.; Murphy, C. J. Solution NMR Analysis of Ligand Environment in Quaternary Ammonium-Terminated Self-Assembled Monolayers on Gold Nanoparticles: The Effect of Surface Curvature and Ligand Structure. *J. Am. Chem. Soc.* 2019, 141 (10), 4316–4327. https://doi.org/10.1021/jacs.8b11445.
- (30) Hens, Z.; Martins, J. C. A Solution NMR Toolbox for Characterizing the Surface Chemistry of Colloidal Nanocrystals. *Chem. Mater.* **2013**, *25* (8), 1211–1221. https://doi.org/10.1021/cm303361s.
- (31) Perera, Y. R.; Hill, R. A.; Fitzkee, N. C. Protein Interactions with Nanoparticle Surfaces: Highlighting Solution NMR Techniques. *Isr. J. Chem.* **2019**, *59* (11–12), 962–979. https://doi.org/10.1002/ijch.201900080.
- (32) Woods, K. E.; Perera, Y. R.; Davidson, M. B.; Wilks, C. A.; Yadav, D. K.; Fitzkee, N. C. Understanding Protein Structure Deformation on the Surface of Gold Nanoparticles of Varying Size. *J. Phys. Chem. C* **2016**, *120* (49), 27944–27953. https://doi.org/10.1021/acs.jpcc.6b08089.
- (33) Wang, A.; Perera, Y. R.; Davidson, M. B.; Fitzkee, N. C. Electrostatic Interactions and Protein Competition Reveal a Dynamic Surface in Gold Nanoparticle–Protein Adsorption. *J. Phys. Chem. C* **2016**, *120* (42), 24231–24239. https://doi.org/10.1021/acs.jpcc.6b08469.
- (34) Li, D.-W.; Xie, M.; Brüschweiler, R. Quantitative Cooperative Binding Model for Intrinsically Disordered Proteins Interacting with Nanomaterials. *J. Am. Chem. Soc.* **2020**, *142* (24), 10730–10738. https://doi.org/10.1021/jacs.0c01885.
- (35) Xie, M.; Li, D.-W.; Yuan, J.; Hansen, A. L.; Brüschweiler, R. Quantitative Binding Behavior of Intrinsically Disordered Proteins to Nanoparticle Surfaces at Individual Residue Level. *Chem. Eur. J.* **2018**, *24* (64), 16997–17001. https://doi.org/10.1002/chem.201804556.
- (36) Xie, M.; Hansen, A. L.; Yuan, J.; Brüschweiler, R. Residue-Specific Interactions of an Intrinsically Disordered Protein with Silica Nanoparticles and Their Quantitative Prediction. *J. Phys. Chem. C* **2016**, *120* (42), 24463–24468. https://doi.org/10.1021/acs.jpcc.6b08213.
- (37) An, Y.; Naik, P.; Slowing, I. I.; Venditti, V. Substrate–Support Interactions Mediate Hydrogenation of Phenolic Compounds by Pd/CeO ₂ Nanorods. *ACS Appl. Nano Mater.* **2020**, *3* (11), 11282–11288. https://doi.org/10.1021/acsanm.0c02381.

- (38) Egner, T. K.; Naik, P.; An, Y.; Venkatesh, A.; Rossini, A. J.; Slowing, I. I.; Venditti, V. 'Surface Contrast' NMR Reveals Non-Innocent Role of Support in Pd/CeO2 Catalyzed Phenol Hydrogenation. *ChemCatChem* **2020**, *12* (16), 4160–4166. https://doi.org/10.1002/cctc.202000608.
- (39) Dalvit, C.; Pevarello, P.; Tatò, M.; Veronesi, M.; Vulpetti, A.; Sundström, M. Identification of Compounds with Binding Affinity to Proteins via Magnetization Transfer from Bulk Water. *J. Biomol. NMR* **2000**, *18* (1), 65–68. https://doi.org/10.1023/a:1008354229396.
- (40) Dalvit, C.; Fogliatto, G.; Stewart, A.; Veronesi, M.; Stockman, B. WaterLOGSY as a Method for Primary NMR Screening: Practical Aspects and Range of Applicability. *J. Biomol. NMR* **2001**, *21* (4), 349–359. https://doi.org/10.1023/A:1013302231549.
- (41) Mayer, M.; Meyer, B. Characterization of Ligand Binding by Saturation Transfer Difference NMR Spectroscopy. *Angew. Chem. Int. Ed.* **1999**, *38* (12), 1784–1788. https://doi.org/10.1002/(SICI)1521-3773(19990614)38:12<1784::AID-ANIE1784>3.0.CO;2-O
- (42) Mayer, M.; Meyer, B. Group Epitope Mapping by Saturation Transfer Difference NMR To Identify Segments of a Ligand in Direct Contact with a Protein Receptor. *J. Am. Chem. Soc.* **2001**, *123* (25), 6108–6117. https://doi.org/10.1021/ja0100120.
- (43) Xu, H.; Casabianca, L. B. Probing Driving Forces for Binding between Nanoparticles and Amino Acids by Saturation-Transfer Difference NMR. *Sci. Rep.* **2020**, *10* (1), 12351. https://doi.org/10.1038/s41598-020-69185-7.
- (44) Xu, H.; Lustig, D.; Casabianca, L. B. 13C Saturation-Transfer Difference (STD)-NMR Experiments Using INEPT Polarization Transfer. *Appl. Magn. Reson.* **2020**, *51* (3), 277–286. https://doi.org/10.1007/s00723-019-01182-0.
- (45) Zhang, Y.; Xu, H.; Casabianca, L. B. Interaction between Cyanine Dye IR-783 and Polystyrene Nanoparticles in Solution. *Magn. Reson. Chem.* **2018**, *56* (11), 1054–1060. https://doi.org/10.1002/mrc.4751.
- (46) Zhang, Y.; Xu, H.; Parsons, A. M.; Casabianca, L. B. Examining Binding to Nanoparticle Surfaces Using Saturation Transfer Difference (STD)-NMR Spectroscopy. *J. Phys. Chem. C* **2017**, *121* (44), 24678–24686. https://doi.org/10.1021/acs.jpcc.7b08828.
- (47) Zhang, Y.; Casabianca, L. B. Probing Amino Acid Interaction with a Polystyrene Nanoparticle Surface Using Saturation-Transfer Difference (STD)-NMR. J. Phys. Chem. Lett. **2018**, *9* (23), 6921–6925. https://doi.org/10.1021/acs.jpclett.8b02785.
- (48) Szczygiel, A.; Timmermans, L.; Fritzinger, B.; Martins, J. C. Widening the View on Dispersant–Pigment Interactions in Colloidal Dispersions with Saturation Transfer Difference NMR Spectroscopy. J. Am. Chem. Soc. **2009**, *131* (49), 17756–17758. https://doi.org/10.1021/ja905637y.
- (49) Fawzi, N. L.; Ying, J.; Ghirlando, R.; Torchia, D. A.; Clore, G. M. Atomic-Resolution Dynamics on the Surface of Amyloid-β Protofibrils Probed by Solution NMR. *Nature* **2011**, *480* (7376), 268–272. https://doi.org/10.1038/nature10577.
- (50) Fawzi, N. L.; Ying, J.; Torchia, D. A.; Clore, G. M. Probing Exchange Kinetics and Atomic Resolution Dynamics in High-Molecular-Weight Complexes Using Dark-State Exchange Saturation Transfer NMR Spectroscopy. *Nat. Protoc.* 2012, 7 (8), 1523–1533. https://doi.org/10.1038/nprot.2012.077.
- (51) Hwang, T. L.; Shaka, A. J. Water Suppression That Works. Excitation Sculpting Using Arbitrary Wave-Forms and Pulsed-Field Gradients. *J. Magn. Reson. A* **1995**, *112* (2), 275–279. https://doi.org/10.1006/jmra.1995.1047.
- (52) Moreno-Villoslada, I.; Jofré, M.; Miranda, V.; González, R.; Sotelo, T.; Hess, S.; Rivas, B. L. PH Dependence of the Interaction between Rhodamine B and the Water-Soluble Poly(Sodium 4-Styrenesulfonate). *J. Phys. Chem. B* **2006**, *110* (24), 11809–11812. https://doi.org/10.1021/jp061457j.
- (53) Nakashima, K.; Duhamel, J.; Winnik, M. A. Photophysical Processes on a Latex Surface:

- Electronic Energy Transfer from Rhodamine Dyes to Malachite Green. *J. Phys. Chem.* **1993**, *97* (41), 10702–10707. https://doi.org/10.1021/j100143a029.
- (54) Moreno-Villoslada, I.; Jofré, M.; Miranda, V.; Chandía, P.; González, R.; Hess, S.; Rivas, B. L.; Elvira, C.; San Román, J.; Shibue, T.; Nishide, H. π-Stacking of Rhodamine B onto Water-Soluble Polymers Containing Aromatic Groups. *Polymer* **2006**, *47* (19), 6496–6500. https://doi.org/10.1016/j.polymer.2006.07.059.

TOC Graphic

